

Central exclusive meson production in proton–proton collisions in ALICE at the LHC

R. Schicker

(for the ALICE Collaboration)

Physikalisches Institut

University Heidelberg

69120 Heidelberg, Germany

E-mail: schicker@physi.uni-heidelberg.de

Central exclusive production at hadron colliders is characterised by the hadronic state produced at or close to midrapidity, and by the two forward scattered protons, or remnants thereof. No particles are produced between the midrapidity system and the forward going beam particles, and such events can hence be identified experimentally by a double-gap topology. At LHC energies, central exclusive production in proton–proton collisions is dominated by pomeron–pomeron fusion. The models to describe such reactions are reviewed, and the ongoing efforts in the ALICE Collaboration to analyse double-gap events taken in Run 2 at the LHC are presented.

Keywords: Central production, double-gap topology, pomeron, diffraction.

1. Diffractive event topologies

In the Regge approach, the hadronic interaction between strongly interacting particles is due to the exchange of trajectories. Such trajectories $\alpha(t)$ parameterise the almost linear dependence between the spin and the mass squared ($t=m^2$) of a particle and its higher spin excitations. A trajectory is characterised by two parameters, the intercept $1+\varepsilon$ and the slope α' , and is expressed as $\alpha(t) = 1+\varepsilon+\alpha't$. In Regge phenomenology, the contribution of a trajectory to the energy behaviour of the total cross section scales as $\sigma_{tot} \propto s^\varepsilon$. For meson trajectories, such as the ρ, ω, a, f , the value of $\varepsilon \sim -0.5$ and the corresponding contributions decrease as function of energy¹. Such a behaviour is seen in the elastic and total hadron-hadron cross section which decrease from threshold up to a centre-of-mass energy $\sqrt{s} \sim 20$ GeV. At higher energies, however, elastic and total hadron-hadron cross sections increase². Within the Regge approach, this increase is attributed to the existence of an additional exchange mechanism in both elastic and inelastic channels, which is referred to as the pomeron trajec-

tory. The characterisation of the bound states underlying the pomeron trajectory, and their possible experimental verification, is a considerable challenge from the theoretical as well as the experimental perspective.

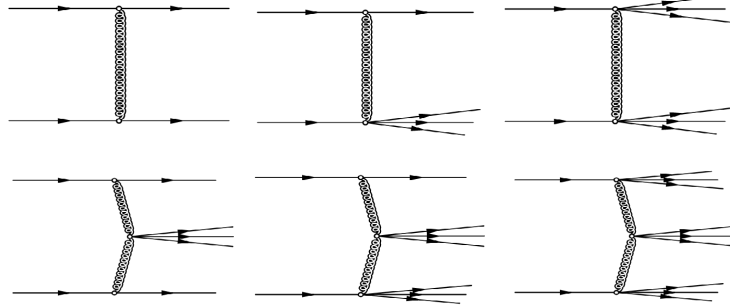


Fig. 1. Top row: Single pomeron elastic scattering (left), and single pomeron inelastic scattering (middle and right). Bottom row: Central exclusive production (left), central production with proton excitation (middle and right).

In the top row of Fig. 1, the diagrams of strong elastic and inelastic scattering due to single pomeron exchange are shown. The corresponding cross sections have been measured at LHC energies by the TOTEM and the ALICE Collaboration, respectively^{3,4}. In the bottom row of Fig. 1, the double-pomeron exchange channel of exclusive production is shown on the left, and central production with proton excitation in the middle and on the right. The universality of pomeron exchange can be tested in these central production channels at high energies, where Regge meson contributions are negligible as compared to the pomeron exchange.

2. The spin structure of the soft pomeron

It is generally agreed that the pomeron exchange carries the vacuum internal quantum numbers of charge $Q = 0$, colour charge $Q_C = 0$, isospin $I = 0$ and charge conjugation $C = 1$. Under intense debate is, however, the spin structure of the pomeron exchange in the nonperturbative regime of QCD, the soft pomeron exchange⁵. In contrast to the vacuum expectation value of spin zero, a vector pomeron exchange has been successfully used to describe elastic proton–proton and proton–antiproton scattering data, as well as production of high- p_T jets and Drell-Yan pairs^{6,7}. In this vector approach, the single pomeron exchange amplitudes of proton–proton and proton–antiproton elastic scattering carry, however, a relative minus sign. By use of the optical theorem, this minus sign propagates into an opposite sign between the proton–proton and proton–antiproton cross section.

Alternatively, a description of the soft pomeron as an effective rank-2 symmetric tensor has been proposed⁸. Here, the meson exchanges of positive and negative charge conjugation are treated as effective tensor and vector exchanges, respectively, with many effective couplings to hadrons derived from experimental data. The single spin asymmetry data of the STAR Collaboration have been analysed with the tensor pomeron model^{9,10}. The results of this analysis disfavour the scalar pomeron, and are in very good agreement with the tensor pomeron. In the analysis of central production of scalar and pseudo-scalar mesons within the vector and tensor pomeron approach, the azimuthal opening angle between the two final-state protons was found to be a sensitive probe for the two approaches⁸.

3. DAMA model of central production

The double-differential cross section $d\sigma/dMdp_T$ for central exclusive meson production shown in the bottom left of Fig. 1 can be derived in a model based on a Dual Amplitude with Mandelstam Analyticity (DAMA)¹¹. For central production, the direct-channel pole decomposition of the DAMA amplitude is relevant¹². In this approach, the pomeron flux in the proton is convoluted with the pomeron-pomeron-meson cross section derived by the optical theorem from the DAMA amplitude¹³. The DAMA amplitude is based on nonlinear, complex trajectories. The imaginary part of the trajectory is related to the decay width of the bound states of the trajectory, and is connected to the almost linear real part by a dispersion relation.

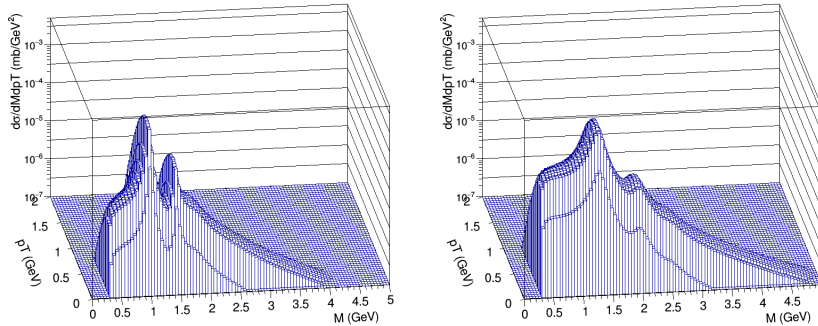


Fig. 2. Central exclusive cross section for resonances on the $f_0(980)$ trajectory (left), and on the $f_2(1270)$ trajectory (right) (Figs. from Ref. 13).

In Fig. 2 the cross section $d\sigma/dMdp_T$ for the resonances on the trajectory of the $f_0(980)$ is shown on the left, and the $f_2(1270)$ on the right.

4. Central exclusive production in ALICE

ALICE consists of a central barrel in the pseudorapidity range $|\eta| < 0.9$, and a forward muon spectrometer¹⁴. An inner tracking system (ITS), composed of silicon pixel, drift and strip detectors, measures the particle tracks in the innermost 6 layers of the central barrel. A cylindrical time projection chamber with a sensitive volume from $r_{\min}=88$ cm to $r_{\max}=250$ cm records track ionisation clusters. The specific Bethe-Bloch ionisation loss is used for particle identification, and the cluster space information is used together with the ITS space points to reconstruct the track momentum. Additional detectors outside of the central barrel are used for trigger purposes, and for classifying the event according to multiplicity. Each of the V0 and AD detectors consists of a pair of plastic scintillators which cover the range $2.8 < \eta < 5.1$, $4.9 < \eta < 6.1$, respectively, and $-3.7 < \eta < -1.7$, $-7.0 < \eta < -4.8$.

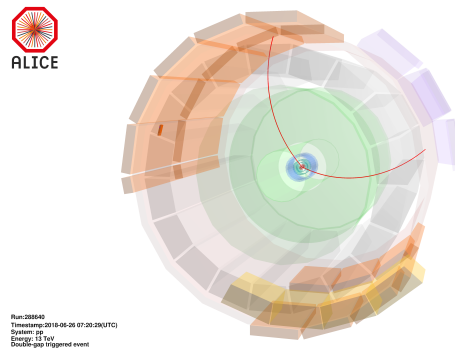


Fig. 3. Double-gap event in the ALICE central barrel.

The double-pomeron events of Fig. 1 consist of particles produced at midrapidity, and of the beam protons, or remnants thereof, at or close to beam rapidity. No particles are produced in between, which yields a rapidity region without particles, known as the gap. This rapidity gap is a signature of central production which can be used for filtering such events from minimum-bias events in the offline analysis, or for tagging at the trigger level. A double-gap event in the ALICE central barrel is shown in Fig. 3.

5. ALICE data on exclusive pion pair production

Exclusive production of $\pi^+\pi^-$ pairs has been studied within the tensor pomeron approach¹⁵. The dipion continuum and pion pairs from decays of scalar $f_0(500)$, $f_0(980)$ and tensor $f_2(1270)$ resonance were considered. The resulting mass distribution is shown in Fig. 4 on the left. Photoproduction of $\rho(770)$ is visible at LHC energies due to the large photon fluxes, shown

in the middle. The uncorrected pion-pair mass distribution measured by ALICE in proton–proton collisions at $\sqrt{s} = 13$ TeV is shown on the right. An analogous analysis has been done for K^+K^- -pairs¹⁶. The ALICE data sample shown in Fig. 4 will be increased in the LHC Run 3 by a factor of about 40. The study of the measured resonances by a Partial Wave Analysis in both the light quark and strangeness sector will become feasible.

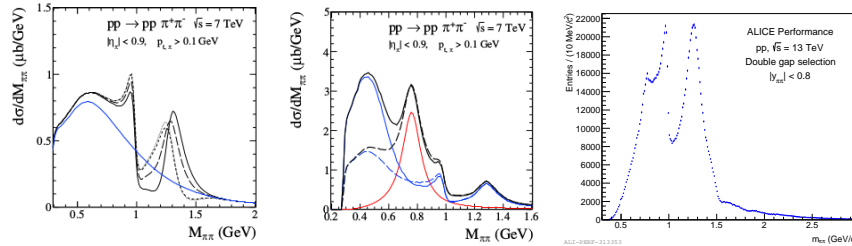


Fig. 4. Model predictions of Ref. 15 for central pion pair mass distribution (left and middle), and pion pair mass distribution measured by ALICE (right).

6. Acknowledgments

This work is partially supported by the German Federal Ministry of Education and Research under promotional reference 05P19VHCA1.

References

1. A. Donnachie, H.G. Dosch, P.V. Landshoff, and O. Nachtmann. *Pomeron physics and QCD*, Camb. Mono. Part. Nucl. Phys. **19** (2002).
2. M. Tanabashi *et al.*, (Part. Data Group), Phys.Rev.D**98**,(2018) 03001.
3. TOTEM Coll., (G. Antchev *et al.*), Eur.Phys.J. **C79**, (2019)no.10,861.
4. ALICE Coll., (B. Abelev *et al.*), Eur.Phys.J. **C73**, (2013) no.6, 2456.
5. C. Ewerz, M. Maniatis, O. Nachtmann, Annals Phys. 342 (2014) 31.
6. A. Donnachie, P.V. Landshoff, Phys.Lett. B727 (2013) 500.
7. A. Donnachie, P.V. Landshoff, Nucl. Phys. B **303** (1988) 634.
8. P. Lebiedowicz, O. Nachtmann, A. Szczurek, Ann. Phys. 344(2014)301.
9. L. Adamczyk *et al.*, STAR Collaboration, Phys. Lett. B **719** (2013) 62.
10. C. Ewerz, P. Lebiedowicz, O. Nachtmann, A. Szczurek, Phys. Lett. B763 (2016) 382.
11. A.J. Bugrij *et al.*, Fortschr. Phys. **21**, (1973) 427.
12. R. Fiore, L. Jenkovszky, R. Schicker, Eur.Phys.J.C**76** (2016), no.1, 38.
13. R. Fiore, L. Jenkovszky, R. Schicker, Eur.Phys.J.C**78** (2018) no.6, 468.
14. ALICE Coll., (B. Abelev *et al.*), Int.J.Mod.Phys. **A29**, (2014)1430044.
15. P. Lebiedowicz, O. Nachtmann, A. Szczurek, Phys.Rev. D93 (2016) no.5, 054015.
16. P. Lebiedowicz, O. Nachtmann, A. Szczurek, Phys.Rev. D98 (2018) 014001.